Entropy-driven demixing in spherocylinder binary mixtures

Hadrien Bosetti and Aurélien Perera
Laboratoire de Physique Théorique des Liquides, Unité associée au CNRS, Université Pierre et Marie Curie, Case Courrier 121, 4 place Jussieu, 75252 Paris Cedex 05, France

(Received 23 August 2000; published 26 January 2001)

The stability of binary fluid mixtures, with respect to a demixing transition, is examined within the framework of the geometrical approximation of the direct correlation for hard nonspherical particles. In this theory, the direct correlation function is essentially written in terms of the geometrical properties of the individual molecules, and those of the overlap region between two different molecules, taken at fixed separation and orientations. Within the present theory, the demixing spinodal line in the (ρ_1,ρ_2) concentration plane is obtained analytically, and shown to be a quadratic function of the total packing fraction and the compositions. The theory is applied herein to binary mixtures of hard spherocylinders in the isotropic phase. Isotropic fluid-fluid demixing can be predicted for a large variety of sizes and aspect ratios, and the necessary condition for entropic demixing is a sufficiently large thickness difference between the two particles that belong to each of the fluids in the mixture. As the theory reduces exactly to the Percus-Yevick approximation for a hard sphere mixture, accordingly it will not predict fluid-fluid demixing for this particular case. Demixing is also forbidden in two other cases; for a mixture of spherocylinders and small spheres, and for mixtures of equally thin spherocylinders. The influence and competition of an ordering instability on the demixing is also examined. The ordering of a fluid will always be displaced toward higher packing fractions by the addition of a nonordering fluid, and in some cases the entropic demixing can dominate the entire fluid range. Although the present theory merges exactly with the correct Onsager limit, it is shown that, for intermediate cases, the results can be significantly different from predictions of Onsager type approaches. These discrepancies are analyzed in particular for the needle plus spherocylinder mixture. Finally, in view of the nature of the theory, it is conjectured that the predicted demixing densities values are rather upper bounds to what should be expected.

DOI: 10.1103/PhysRevE.63.021206 PACS number(s): 61.20.−p

I. INTRODUCTION

The entropy driven phase transition in hard core molecular fluids has been a well established phenomenon since the pioneering work of Onsager [1], who showed that an isotropic-nematic phase transition could occur in a fluid of infinitely long spherocylinder like shaped molecules, induced solely by excluded volume effects. One would then be naturally led to ask whether entropy driven isotropic phase separation in hard core fluids could also occur under appropriate conditions. However, one of the major analytical theories in liquid state physics, the Percus-Yevick theory, outruled such phase separation for additive hard sphere mixtures [2]. About a decade ago, Biben and Hansen [3] showed that closure relations more elaborate than the Percus-Yevick approximation, could in principle predict such a phase separation for hard sphere mixtures when the size ratio exceeds 4. However, they found that the predicted spinodals depend severely on the closure relation. For example, for a size ratio 5 and a packing fraction of the small spheres of $\eta_S=0.4$, the hypernetted chain approximation predicts phase separation at a large sphere packing fraction $\eta_L=0.124$ [4]; however, the more accurate Rogers-Young closure predicts a larger value of $\eta_L\approx 0.32$ [3], and surprisingly, another accurate closure, the Ballone-Pastore-Galli-Gazzillo (BPGG) closure, predicts no phase separation [3] in this case. Nevertheless, their finding opened a way to several investigations on the subject, mostly focused on hard spheres. More recent work cast some doubt on whether such entropy driven phase separation actually occurs in hard spheres mixtures in the fluid region, particularly for the large spheres. Computer simulations are meeting a real challenge on this ground, and to date no conclusive results have been proven, although the general consensus is that large spheres are more likely to form some amorphous crystalline phase before the phase separation actually occurs [5,6].

An alternative system that seems worth considering is a mixture of nonspherical hard core molecules. On this subject, however, almost nothing is known from integral equations such as the Percus Yevick theory, although such an approximation has been shown to be solvable and reliable, for pure fluids only. Here, one must rely solely on density functional theories, and eventually on computer simulations. Among all the convex bodies, spherocylinders have a place of choice, as they have been abundantly studied by computer simulations. When compared with hard ellipsoids, they form a more realistic class of model for liquid crystals, as they can exhibit smectic phases, in addition to nematic phases. The entire phase diagram for a single spherocylinder fluid was recently mapped by computer simulations [7]. This type of fluid was also studied by integral equations techniques [8].

For mixtures, Dijkstra and van Roij calculated the phase diagram of needles mixed with spherocylinders [6], and predicted that phase separation does occur, in rather close agreement with Onsager type density functional theories based on simplified second virial coefficients. On the theoretical side, most approaches have been based on second virial coefficient approximations of the Helmholtz free energy [9–11]. Such approximations merge with the Onsager theory [1], which is valid in the limit of low density and elongated particles. In principle, one could envisage a rescaled approach

of such an approximation where, while the excluded volume would be limited to the second virial coefficient, the density effects could be considered at the level of the Percus-Yevick theory. Indeed, such approaches have already been used for quite accurately predicting the entropy driven isotropic-nematic phase transition in hard core fluids [12], and could, in principle, be extended to the case of mixtures. However, it would be more desirable to have an approximate theory which goes beyond both the Percus-Yevick and the Onsager approaches. The only case where this goal have been applied successfully is the hard cubes mixtures [13]. The theoretical predictions were compared with lattice simulations [14] both of which predict phase separation in these toy fluid models.

In the present work, we would like to consider the problem of entropy driven phase separation in the light of the geometrical approximation for the direct correlation function (GADCF) that was proposed earlier [15]. The direct correlation function (DCF) plays a fundamental role in theories of liquids, mainly through the Ornstein-Zernike equation. This is theoretically more appealing than the pair correlation function, because it has the same range as the pair interaction, and, in particular, remains short ranged at the critical point. For hard core particles, this range is strictly limited to the spatial region where two particles overlap. The major drawback, however, is that the DCF is not a measurable quantity, as opposed to the pair correlation function. This is quite a severe handicap when considering computer simulations. The GADCF gives a physical grasp to this quantity by postulating that the DCF of any fluid of hard particles can be expressed in terms of the geometrical overlap between the molecules, with all the density dependence appearing only in form of prefactors. Such a formulation is particularly convenient for mixtures, as the only requirement is a knowledge of the geometrical properties of individual constituents. The GADCF has been tested for single fluids of a variety of convex bodies, such as ellipsoids and spherocylinders [15] and cutspheres [16], and has been extended to nonconvex bodies such as hard sphere chains [17]. It has been quite successful in predicting the pressures, structure, and orientational properties of this type of fluids, both in three and two dimensions [18]. The GADCF has two interesting properties. First, it reduces exactly to the Percus-Yevick (PY) approximation for hard spheres. Second, in the low density limit, it reduces to the Mayer function, and hence is reduced to the Onsager theory for very elongated particles. In view of the first property, it is not obvious at all that the GADCF should be suited to study entropic phase separation, since the PY theory does not predict entropic demixing. However, because it is able to predict the orientational instability of liquid crystals, in rather good agreement with the hypernetted chain (HNC) approximation, as opposed to the PY approximation, one is led to believe that the GADCF may incorporate a better description of the excluded volume effects.

The remainder of this paper is divided as follows. In Sec. II we will first expose the general theoretical frame for correlation functions of nonspherical molecules, and particularly the relation to the demixing spinodal. The GADCF is then introduced explicitly for mixtures, and we show that the demixing spinodal can be cast in a simple analytical form. In Sec. III, we consider several particular cases of mixtures, and compare the GADCF with Onsager type approaches and available computer experiments. In Sec. IV we give our conclusions and future expectations about the GADCF for mixtures.

II. THEORY

We consider a binary mixture of hard core convex bodies in the isotropic fluid phase. The theory below is independent of any particular choice for the convex bodies. In Sec. III, we will explicitly consider spherocylindrical molecules.

The partial number densities are noted ρ_1 and ρ_2 ($\rho_i = N_i/V$), and the total density is $\rho = \rho_1 + \rho_2$. The fraction (or composition) of each specie is defined by $x_\alpha = \rho_\alpha/\rho$, and the packing fraction is defined as $\eta_\alpha = \rho_\alpha V_\alpha$ ($\alpha = 1$ and 2), where V_α is the volume of the molecule of specie α. Being a convex body, each molecule of of the fluid component α is then entirely defined by the three geometrical properties associated with its shape, which are the volume V_α, the surface S_α, and the mean radius $R_{m\alpha}$. We will further restrict the symmetry of the molecule to uniaxial, such that the orientation of any molecule i is specified by the unit vector $\hat{u}_i$ with angles (θ_i, ϕ_i) in the lab fixed frame. The structural properties of the mixture can be described by the partial pair distribution functions $g_{\alpha\beta}(12)$ and the partial pair direct correlations $c_{\alpha\beta}(12)$, where (1,2) stands for $(\vec{r}_{12}, \hat{u}_1, \hat{u}_2)$, and $\vec{r}_{12}$ is the vector connecting the centers of mass of the two molecules 1 and 2, belonging to species α and β, respectively. For nonspherical molecules, these correlation functions can be conveniently expanded in the isotropic phase in appropriate basis which accounts for the symmetry of the phase,

$$t_{\alpha\beta}(12) = \sum_{mnl} t^{mnl}_{\alpha\beta}(r) \Phi^{mnl}(\hat{r}, \hat{u}_1, \hat{u}_2), \tag{1a}$$

where $t(12)$ can be either of $c(12)$ or $g(12)$. The rotational invariant Φ^{mnl} is expressed in terms of spherical harmonics and carries all the information on the vector part of the property $t_{\alpha\beta}(12)$, while the expansion coefficients $t^{mn}_{\alpha\beta}(r)$ contain only the radial dependence. Below we recall the expression of the rotational invariants for the isotropic phase [19], which are independent of the specie specifications (α, β), and which are written in terms the generalized spherical harmonics $R^m_{\mu 0}(\hat{u})$ and the $3-j$ symbols as

$$\Phi^{mnl}(12) = f^{mnl} \sum_{\mu\nu\lambda} \begin{pmatrix} m & n & l \\ \mu & \nu & \lambda \end{pmatrix} R^m_{\mu 0}(\hat{u}_1) R^n_{\nu 0}(\hat{u}_2) R^l_{\lambda 0}(\hat{r}). \tag{1b}$$

We will consider the so called ''Blum choice'' for the coefficient $f^{mnl} = \sqrt{(2m+1)(2n+1)}$ which is consistent with a convenient matricial rearrangement of the Ornstein-Zernike equation [19,20].

The theoretical goal is then to accurately compute $t^{mnl}_{\alpha\beta}(r)$'s. Some of the $t^{mnl}_{\alpha\beta}(r)$'s are particularly meaningful. For example, it can shown be that $t^{000}_{\alpha\beta}(r)$, which is the angle average of $t_{\alpha\beta}(12)$, can be related to thermodynamic prop-

erties such as the pressure of the isothermal compressibility, whereas $t_{\alpha\beta}^{110}$ is related to the dielectric constant [21] and $t_{\alpha\beta}^{220}$ can be related to the orientational stability of the fluid [22]. Usually, these coefficients are computed within the integral equation formalism, with a great deal of numerical effort. The geometrical approximation of the direct correlation function [15], that we shall recall below, allows a much simplified route to compute any of the $c_{\alpha\beta}^{mnl}(r)$ *independently of the other* (mnl) *values*, and with minimal numerical effort. Fortunately, for our concern here, we need not compute the entire r dependence of such expansion coefficients, and we shall see that a knowledge of the zero moment of the Fourier transform of these functions $\tilde{c}_{\alpha\beta}^{mnl}(k=0)$ will be sufficient to gather sufficient information on the location of the fluid-fluid phase separation spinodal line.

A. Density correlations and spinodals

Statistical mechanics relates the convexity of the free energy to the mechanical stability of the phase, which is then delimited by a spinodal line. As this line is approached, large concentration fluctuations will occur, rendering the actual phase instable. The correlation range of these fluctuations is directly related to the long range behavior of density correlation functions $g_{\alpha\beta}(12)$, or equivalently $h_{\alpha\beta}(12) = g_{\alpha\beta}(12) - 1$. The approach of the spinodal (or phase boundary) line can be then monitored through the $k \to 0$ behavior of the Fourier transforms of these functions $\tilde{h}_{\alpha\beta}(12)$, which diverge exactly at the spinodal line (k is the inverse wavelength). There are two ways one can seek for the spinodal. One possible way is to look at the relation between the thermodynamical variables that control the stability of the phase and the microscopic correlations that are related to them. For example, the convexity of the Gibbs free energy per particle G/N is related to the partial structure factors $\hat{S}_{\alpha\beta}(k) = \sqrt{x_\alpha x_\beta}[\delta_{\alpha\beta} + \sqrt{x_\alpha x_\beta}\tilde{h}_{\alpha\beta}^{000}(k)]$ through the relation [23,24]

$$\left(\frac{\partial^2 G/(Nk_BT)}{\partial x_1^2}\right)_{N,P,T} = \frac{1}{\lim_{k\to 0}[x_1^2\hat{S}_{22}(k) + x_2^2\hat{S}_{11}(k) - 2x_1x_2\hat{S}_{12}(k)]}. \tag{2}$$

The divergence of $\hat{S}_{\alpha\beta}(k \to 0)$ will then signal the enhancement in concentration fluctuation and the change in curvature (loss of convexity) in G. Alternatively, the spinodal line can be detected directly through the Ornstein-Zernike (OZ) equation at $k=0$. In the Fourier space, this equation reads [21]

$$\tilde{h}_{\alpha\beta}(12) = \tilde{c}_{\alpha\beta}(12) + \frac{1}{4\pi}\sum_\gamma \rho_\gamma \int d\hat{u}_3 \tilde{h}_{\alpha\gamma}(13)\tilde{c}_{\gamma\beta}(32), \tag{3}$$

where (12) stands now for $(\vec{k}, \hat{u}_1, \hat{u}_2)$. Upon expansion of the functions in rotational invariants, and carrying out the angular integral, the OZ equation can be written solely in terms of the Fourier-Hankel transforms of the expansion coefficients $\tilde{h}_{\alpha\beta}^{mnl}(k)$ and $\tilde{c}_{\alpha\beta}^{mnl}(k)$, which are defined by

$$\tilde{h}_{\alpha\beta}^{mnl}(k) = 4\pi(-1)^l \int_0^\infty dr r^2 h_{\alpha\beta}^{mnl}(r) j_l(kr), \tag{4}$$

where $j_l(x)$ is the spherical Bessel function of order l. A similar definition also holds for the transform of the DCF.

As we are interested in the $k=0$ limit, using the mathematical property of the Bessel function, $\lim_{x\to 0} j_l(x) \approx x^l$, we see from Eq. (4) that, if the expansion coefficients $h_{\alpha\beta}^{mnl}(r)$ are well behaved short range functions, then only the $l=0$ terms will remain in the $k=0$ limit. This applies for any thermodynamic state that is not on the spinodal line. In the $k=0$ limit, the OZ equation decouples nicely into the following form:

$$\tilde{h}_{\alpha\beta}^{mm0}(0) = \tilde{c}_{\alpha\beta}^{mm0}(0) + \frac{1}{\sqrt{2m+1}}\sum_\gamma \rho_\gamma \tilde{h}_{\alpha\gamma}^{mm0}(0)\tilde{c}_{\gamma\beta}^{mm0}(0). \tag{5}$$

This equation can be further cast into a matricial form by introducing the matrices $\tilde{\mathbf{H}}_m$ and $\tilde{\mathbf{C}}_m$, whose elements are defined by

$$\tilde{H}_{\alpha\beta}^{(m)} = \sqrt{\rho_\alpha\rho_\beta}\,\frac{\tilde{h}_{\alpha\beta}^{mm0}(0)}{\sqrt{2m+1}}, \qquad \tilde{C}_{\alpha\beta}^{(m)} = \sqrt{\rho_\alpha\rho_\beta}\,\frac{\tilde{c}_{\alpha\beta}^{mm0}(0)}{\sqrt{2m+1}}. \tag{6}$$

Then, the OZ equation in the $k=0$ limit is simply a matricial product:

$$(\mathbf{I} + \tilde{\mathbf{H}}_m)(\mathbf{I} - \tilde{\mathbf{C}}_m) = \mathbf{I}. \tag{7}$$

It can be seen that, for $m=0$, the first matrix in the product above is simply related to the matrix of the partial structure factors that appear in Eq. (2) by the following expression

$$\hat{S}_{\alpha\beta}(k=0) = \sqrt{x_\alpha x_\beta}(\delta_{\alpha\beta} + \tilde{H}_{\alpha\beta}^{(0)}). \tag{8}$$

Equation (7) allows us to compare the phase separation spinodal with that of the liquid-vapor spinodal for a pure fluid. In the latter case, the OZ relation can be written as $[1 + \rho\tilde{h}(0)][1 - \rho\tilde{c}(0)] = 1$, in terms of the correlation functions of the simple fluid. As the spinodal line is approached, $\tilde{h}(0)$ will tend to diverge, due to the building of long range density correlations in $h(r)$. But the direct correlation function remains finite, even at the critical point; thus the divergence of $\tilde{h}(0)$ can be monitored by the limit $1 - \rho\tilde{c}(0) \to 0$. In the case of a mixture, we see that the condition

$$\det(\mathbf{I} - \tilde{\mathbf{C}}_m) = 0 \tag{9}$$

can be considered as the alternative definition of the spinodal. This is the definition that we will be using throughout this work. It is important to see that the matrix elements $\tilde{C}^{(m)}_{\alpha\beta}$ remain finite on the spinodal line, and that any divergence in $\tilde{H}^{(m)}_{\alpha\beta}$ will appear in Eq. (7) through the condition in Eq. (9).

We see that Eq. (9) also contains information about the orientational spinodal, as opposed to the case of spherical particles fluid mixture. Indeed, condition (9) can be also satisfied for $m \neq 0$. Hence there can be competition between an isotropic spinodal (like a disordered phase separation) and the appearance of an orientational spinodal for $m \neq 0$. In particular, the orientational spinodal for isotropic-nematic transition occurs for $m=2$ [22].

The studies of phase separation based on Eq. (9), which are focussed on the stability of the mixture, are quite different in spirit from those based on approximations of the free energy, which need no reference to structural properties. They are also more demanding, as an accurate description of these properties is a prerequisite.

In order to apply the above formalism to actual phase separation, we need to compute the correlation functions for explicit cases. This can be achieved, for example, by integral equation techniques for mixtures of nonspherical particles. However, it is quite a cumbersome route to obtain these functions, as it is already quite numerically involved for the single component case. Moreover, the integral equations are known to be less reliable close to the phase separation when many body effects become more important.

One alternative route is the geometrical approximation of the direct correlation function which has been shown to be quite accurate in computing the thermodynamical properties and the DCF for simple fluids in many cases [15,18]. The general formalism was presented in Ref. [15]. We recall and detail the theory in the present context, with explicit application for binary mixtures.

B. Geometrical approximation of the direct correlation function of mixtures

The pair direct correlation is approximated by the following expression, which involves the geometrical properties of the overlap region of two convex bodies:

$$c_{\alpha\beta}(12) = -\chi_V \Delta V_{\alpha\beta}(12) - \chi_S \Delta S_{\alpha\beta}(12) + \chi_0 F_{\alpha\beta}(12), \tag{10}$$

where $\Delta V_{\alpha\beta}(12)$ is the volume of the overlap between molecule 1 of specie α and molecule 2 of specie β, $\Delta S_{\alpha\beta}(12)$ is the surface of that overlap, and $F_{\alpha\beta}(12) = \exp[-\phi_{\alpha\beta}(12)/(k_B T)] - 1$ is the Mayer function [$\phi_{\alpha\beta}(12)$ is the interaction energy between the two molecules, which is simply in the present case infinity when two particles overlap and zero when they do not]. The coefficients χ_V, χ_S, and χ_0 depend only on the partial densities and the geometrical characteristics of the two molecules through the following parameters which are the elementary variables of the scaled particle theory (SPT) [2],

$$\eta_i = \sum_\alpha \rho_\alpha \xi_i^{(\alpha)}, \quad i = 0, 1, 2, \text{ and } 3, \tag{11}$$

where the sum is carried over all the species α in the mixture, and the ξ parameters are the fundamental measures of the SPT associated with the mean radius, the surface and the volume of each convex body α, through the notation $\xi_0 = 1$, $\xi_1^{(\alpha)} = R_{m;\alpha}$, $\xi_2^{(\alpha)} = S_\alpha$, and $\xi_3^{(\alpha)} = V_\alpha$.

The expressions for the coefficients χ in Eq. (10) were derived in Ref. [15] as combinations of second order partial derivatives of the SPT free energy density, and here we recall their explicit expressions:

$$\chi_V = \frac{\eta_0}{(1-\eta_3)^2} + \frac{2\eta_1\eta_2}{(1-\eta_3)^3} + \frac{1}{4\pi}\frac{\eta_2^3}{(1-\eta_3)^4},$$

$$\chi_S = \frac{\eta_1}{(1-\eta_3)^2} + \frac{1}{4\pi}\frac{\eta_2^2}{(1-\eta_3)^3} + \frac{1}{4\pi}\frac{\gamma_{\alpha\beta}\eta_2}{(1-\eta_3)^2}, \tag{12}$$

$$\chi_0 = \frac{1}{1-\eta_3} + \gamma_{\alpha\beta}\frac{R_{m\alpha}R_{m\beta}}{R_{m\alpha}+R_{m\beta}}\frac{\eta_2}{(1-\eta_3)^2}.$$

The coefficients $\gamma_{\alpha\beta}$ have been tailored in order that the expression for the DCF gives the correct SPT isothermal compressibility [15]. They also ensure that the DCF, as defined in Eq. (10), reduces exactly to the PY expression for hard spheres mixtures. We note that the last two coefficients actually depend on the pair of molecules (α,β) through these coefficients, which are given by

$$\gamma_{\alpha\beta} = \frac{\left[R_{m\alpha}V_\beta + R_{m\beta}V_\alpha + \frac{S_\alpha S_\beta}{4\pi}\right](R_{m\alpha}+R_{m\beta})}{\frac{S_\alpha V_\beta + S_\beta V_\alpha}{4\pi} + 2R_{m\alpha}R_{m\beta}B_{2;\alpha\beta}}, \tag{13}$$

where $B_{2;\alpha\beta}$ is the second virial coefficient associated with the pair (α,β). For convex bodies, there is simple a analytical expression for this coefficient [25]:

$$B_{2;\alpha\beta} = (V_\alpha + V_\beta + S_\alpha R_{m\beta} + S_\beta R_{m\alpha})/2. \tag{14}$$

Equations (10)–(14) complete the prescription of the GADCF.

The overlap volumes and surfaces can be written simply as convolution products of the elementary weight functions associated with the volume and surface of each convex body [15]. Explicit analytical expressions for the expansion coefficients of these terms were given in Ref. [15] for different geometries. The Mayer functions expansion coefficients, on the other hand, must be calculated by a numerical computation of the angular integrations, as outlined, for example, in Ref. [22]. For the present problem, however, we do not explicitly need expansion coefficients, but rather their $k=0$ values for the more important of them, namely, for $m=0$ and for $m=2$.

It is not difficult to realize that the angular average of the overlap regions, when integrated over all separations lead to the simple combinations

$$\Delta\tilde{V}^{000}_{\alpha\beta}(k=0) = \left\langle \int d\vec{r}\,\Delta V_{\alpha\beta}(12) \right\rangle_{\hat{u}_1,\hat{u}_2} = V_\alpha V_\beta, \tag{15a}$$

$$\Delta\tilde{V}^{mnl}_{\alpha\beta}(k=0)=0 \quad (m,n,l)\neq(0,0,0),$$

$$\Delta\tilde{S}^{000}_{\alpha\beta}(k=0)=\left\langle \int d\vec{r}\Delta S_{\alpha\beta}(12)\right\rangle_{\hat{u}_1,\hat{u}_2}=S_\alpha V_\beta+S_\beta V_\alpha, \tag{15b}$$

$$\Delta\tilde{S}^{mnl}_{\alpha\beta}(k=0)=0, \quad (m,n,l)\neq(0,0,0).$$

These results can be rigorously derived from the fact that the overlap volume is the convolution of the individual volume weights, and the fact that the overlap surface is the sum of the convolution of the individual volume and surface weights for each pair of bodies [15]. The most remarkable feature is that neither expressions have anisotropic contributions, which is also intuitive.

For the Mayer function $F_{\alpha\beta}(12)$, the angular and radial average is quite simply the excluded volume between the two bodies, which is known analytically for any convex body to be twice the corresponding second virial coefficient [25]:

$$F^{000}_{\alpha\beta}(k=0)=-2B_{2;\alpha\beta}. \tag{16}$$

There is also an anisotropic contribution to the Mayer expansion coefficients in the $k=0$ limit. These terms are known analytically for few convex bodies [25]. For spherocylinders it can be expressed simply in terms of the spherical cap diameter σ and the cylinder length L for each individual specie as

$$F^{220}_{\alpha\beta}=\frac{\sqrt{5}\pi}{32}L_\alpha L_\beta(\sigma_\alpha+\sigma_\beta). \tag{17}$$

[The factor $\sqrt{5}$ in expression above comes from the choice in Eq. (1b) for f^{220}].

We note that the anisotropy of the DCF for the GADCF in the $k=0$ limit comes entirely from the Mayer function. Thus $k=0$ orientational contributions to the GADCF will be treated at the second virial approximation, in the spirit of the Onsager type approach. However, we note here that this contribution is rescaled by a density dependent term χ_0 which is nontrivial. We note in particular that χ_0 is not the PY hard sphere compressibility term, which is often used as a prefactor to the Mayer function, for example in effective liquid type approximation such as SCELA [12]. The present approach predicts the orientational spinodal of simple fluids, in close agreement with the HNC approximation [15].

C. Explicit expressions for the demixing spinodal for a two-component mixture

It turns out that inserting the GADCF expression given in Eq. (10) into Eq. (9), together with the different terms from Eqs. (12)–(16), the resulting calculation can be carried explicitly for a two component system. In this case the relevant partial DCF are $c_{11}(12)$, $c_{12}(12)$, and $c_{22}(12)$.

The determinant in Eq. (9) is then

$$\left(1-\rho_1\frac{\tilde{c}^{mm0}_{11}(0)}{\sqrt{2m+1}}\right)\left(1-\rho_2\frac{\tilde{c}^{mm0}_{22}(0)}{\sqrt{2m+1}}\right)-\rho_1\rho_2\frac{[\tilde{c}^{mm0}_{12}(0)]^2}{2m+1}=0. \tag{18}$$

For $m=0$ one obtains very simple quadratic expressions for the spinodal in terms of the partial density variables. This spinodal can be written either as a function of the two packing fractions η_1 and η_2, or in terms of the variables (ρ,x_2). Other choices are possible, but we consider the ones above as particularly relevant to our presentation.

In the following notation, and for the remainder of this paper we will implicitly consider specie 1 as the ''solvent'' and specie 2 as the ''solute.'' We then consider the demixing of the fluid when fluid 2 is added progressively to fluid 1.

For the choice of variables (η_2,η_1) for Eq. (18) and $m=0$, after some algebra we obtain the following expression, which is symmetrical in both variables:

$$A_{22}\eta_2^2+A_{11}\eta_1^2+A_{12}\eta_1\eta_2+A_2\eta_2+A_1\eta_1+A_0=0, \tag{19a}$$

where the coefficients are given by

$$A_{\alpha\alpha}=V_\beta^2(4\pi V_\alpha^2+S_\alpha^3-8\pi V_\alpha S_\alpha R_{m\alpha}) \quad \alpha=1,2 \ \ (\beta=2,1)$$

$$A_{12}=V_1V_2[S_1S_2(S_1+S_2)+8\pi(V_1-S_1R_{m1})(V_2-S_2R_{m2})-4\pi((S_1R_{m2})^2+(S_2R_{m1})^2)],$$

$$A_\alpha=-8V_\alpha V_\beta^2\pi(V_\alpha-S_\alpha R_{m\alpha}), \quad \alpha=1,2 \ \ (\beta=2,1), \tag{19b}$$

$$A_0=-4\pi V_1^2V_2^2.$$

For the other choice of variables (ρ,x_2) we obtain

$$\rho^2(B_{22}x_2^2+B_{21}x_2+B_{20})+\rho(B_{11}x_2+B_{10})+B_0=0, \tag{20a}$$

with the coefficients given by

$$B_{22}=(S_1+S_2)(S_1-S_2)^2+4\pi(V1-V2)^2+8\pi(V1-V2)\times(S_2R_{m2}-S_1R_{m1})+4\pi(S_1R_{m2}-S_2R_{m1})^2,$$

$$B_{21}=S_1S_2(S_1+S_2)-2S_1^3+8\pi V_1(V_2-V_1+2S_1R_{m1}-S_2R_{m2})-4\pi(S_1R_{m2}-S_2R_{m1})^2-8\pi V_2S_1R_{m1},$$

$$B_{20}=4\pi V_1^2+S_1^3-8\pi V_1S_1R_{m1},$$

$$B_{11}=8\pi(V_1-V_2-S_1R_{m1}+S_2R_{m2}),$$

$$B_{10}=-8\pi(V_1-S_1R_{m1}),$$

$$B_0=4\pi. \tag{20b}$$

From these expressions, one can solve trivially for η_1 as a function of η_2, or equivalently for ρ as a function of x_2:

$$\eta_1(\eta_2)=\frac{-(A_{12}\eta_2+A_2)-\sqrt{(A_{12}\eta_2+A_2)^2-4A_{22}(A_{11}\eta_1^2+A_1\eta_1+A_0)}}{2A_{22}}, \tag{21}$$

$$\rho_S(x_2)=\frac{-(B_{11}x_2+B_{10})-\sqrt{(B_{11}x_2+B_{10})^2-16\pi(B_{22}x_2^2+B_{21}x_2+B_{20})}}{2(B_{22}x_2^2+B_{21}x_2+B_{20})}. \tag{22}$$

These expressions are particularly interesting as they can be inserted into the SPT pressure, which we recall is consistent with the DCF given in Eq. (10) [15]. This expression is explicitly given by

$$\frac{P}{k_BT}=\frac{\eta_0}{1-\eta_3}+\frac{\eta_1\eta_2}{(1-\eta_3)^2}+\frac{1}{12\pi}\frac{\eta_2^3}{(1-\eta_3)^3}. \tag{23}$$

From Eqs. (20) and (21) one can then compute the pressure along the spinodal line.

One can also compute the isothermal compressibility which for a two component system can be written in terms of the partial DCF as [21]

$$\frac{\chi_T^0}{\chi_T}=1-\rho[x_1^2\tilde{c}_{11}^{000}(0)+x_2^2\tilde{c}_{22}^{000}(0)+2x_1x_2\tilde{c}_{12}^{000}(0)], \tag{24}$$

where $\chi_T^0=1/(\rho k_BT)$ is related to the ideal gas compressibility. We note immediately that, unlike the single fluid case for which the divergence of the compressibility is associated with the equivalent of Eq. (9) [that is, $1-\rho\tilde{c}(0)=0$], for mixtures this is not necessarily the case. Indeed, for a two component system, the expression for the inverse of the isothermal compressibility is quite different from Eq. (18).

It is possible to derive the expression for the SPT chemical potentials from the thermodynamic identity $\mu_i=\partial\phi/\partial\rho_i$ ($i=1$, and 2), where ϕ is the SPT free energy density [2]. However, it was shown in Ref. [15] that, while the SPT pressure is consistent with Eq. (10), in the sense that it can be derived from direct integration of the compressibility, the SPT free energy is not consistent with the GADCF, mainly due to the loss of information when arriving at expression (10). Building a coexistence curve from the SPT free energy will not necessarily be the same operation as building it from the DCF. More importantly, such a coexistence curve will not necessarily coincide with the spinodal derived from the DCF at the critical consolute points. For these reasons, we will restrict ourselves here to the spinodal curve.

We briefly examine the case of an orientational spinodal. Unfortunately, it is not possible to derive a simple expression for this spinodal condition when $m=2$ in Eq. (9). The resulting expressions are still polynomials in partial densities, but of degree 6 in the density variables. Hence these expressions are of no use for simple solutions such as Eqs. (21) and (22). We will solve these equations numerically in Sec. III.

We are now in position to study entropic phase separation for particular cases. Before we do this, it is instructive to compare our expressions to those derived in Onsager type approaches, where the DCF is reduced to the Mayer function.

D. Comparison with the Onsager limit

It is important to examine the Onsager limit, as almost all theoretical results on the the present topic are based on this type of approximation. In particular we wish to show explicitly that the theory exposed in Sec. II C reduces to the Onsager limit. This limit is appropriate to study cases where the particles are ''very'' elongated, and subsequently restricted to the very low density region.

There are two levels of approximation in this type of theory. The first one consists of truncating the excess free energy at the second order in density, neglecting virial coefficients higher than 2. This is strictly equivalent to reducing the direct correlation function to the Mayer function [e.g., Eqs. (16) and (17)] to which it is rigously equal in the zero density ideal gas limit. From Eqs. (12), we see that, taking the low density limit, only the term $\chi_0=1$ will remain as $\rho\rightarrow 0$. Therefore, from Eq. (10), we see that our expressions for the partial DCF satisfy this limit correctly. Most theories are based on this type of approximation, which seems reasonable when the density is very low, *but not necessarily when the particles are very elongated*, unless we state explicitly what is meant by that. In what follows, we will refer to this level of approximation as the second virial coefficient Onsager approximation (SVCOA).

The second level of approximation is precisely to take the infinite limit of size ratio. Onsager did that for spherocylindrical particles, of diameter σ and cylinder length L, and in the limit $L/\sigma\rightarrow\infty$ he neglected the spherical caps, retaining in the second virial coefficient the first term remaining in that limit. The essential purpose was to demonstrate that excluded volume effects alone can drive an isotropic to nematic transition, and that was a pioneering breakthrough [1]. We will refer to such an approximation as a full Onsager approximation (FOA).

When coming to mixtures, we realize that, unless we take both components to be extremely elongated, this limit is quite unrealistic, at least for the smallest component. In Sec. III we will examine the particular case of a needle and rod mixture, for various rod sizes, and we will show that there can be large differences between the two limits. Clearly, as this second case is only a limiting case of the second virial approximation, our theory is also able to correctly reproduce this limit.

The pressure in the Onsager approximation is given by a second order expansion in density, similarly to the free en-

ergy, and is simply written in terms of the second virial coefficients as

$$\frac{P_O}{k_B T}=\rho+\rho^2(x_1^2 B_{2;11}+x_2^2 B_{2;22}+2x_1x_2 B_{2;12}). \quad (25)$$

For the FOA, the second virial coefficients are simply taken in the $L/\sigma\to\infty$ [10].

Finally, there is one case that we would like to examine closely, which is the demixing of hard spheres in the second virial approximation. We show in the Appendix that there is indeed a possibility for demixing hard spheres when the size ratio exceeds 2.95. In view of computer simulation results that predict this demixing to occur (if it occurs at all) around size ratios of 10, we can appreciate the level of approximation that is made by retaining only second order terms in the free energy. As the PY theory contains the Mayer function exactly (and hence the second virial), one may ask how this contribution is destroyed by the approximated higher order terms. Furthermore, as the GADCF is built on the PY approximation, one may wonder why it is more appropriate for predicting orientational ordering instability. We believe that this could be due to the fact that the overlap volume and surface terms that are dominant [Eq. (10)] do not contribute to the anisotropic part of the DCF in the $k=0$ limit. In this limit, it is only the Mayer function that gives a nonvanishing contribution. Consequently, the PY approximation must incorporate the density dependence of the prefactor into a Mayer function that is weaker than χ_0.

III. RESULTS: ENTROPIC DEMIXING IN SPHEROCYLINDERS MIXTURES

We now consider a two fluid mixture of spherocylinders, each specified by a diameter σ_α and a cylinder length L_α ($\alpha=1,2$). For spherocylinders, the volume, surface, and mean radius are given by [25]

$$V_\alpha=\frac{\pi}{12}(3L_\alpha+2\sigma_\alpha)\sigma_\alpha^2,$$

$$S_\alpha=\pi(L_\alpha+\sigma_\alpha)\sigma_\alpha, \quad (26)$$

$$R_{m\alpha}=\frac{1}{4}(L+2\sigma_\alpha).$$

The second virial coefficients are then given by Eq. (14).

The densities can be reduced by the cube of one of the diameters, which we choose arbitrarily to be that of specie 1. This is equivalent of taking $\sigma_1^*=1$. Therefore, in all that follows, we choose specie 1, with the smallest diameter as the ''solvent.'' This choice of solvent and solute is arbitrary, and does not affect the generality of the discussion throughout this section.

The reduced partial densities are then defined by $\rho_\alpha=\rho_\alpha\sigma_1^3$, where the same notation has been used for the reduced variables in order to avoid notational burden. Similarly, in what follows we also keep the notation $\sigma_2=\sigma_2/\sigma_1$ and $L_\alpha=L_\alpha/\sigma_1$. The volume, surface, and radius will also be reduced by σ_1^n, with $n=3$, 2, and 1, respectively.

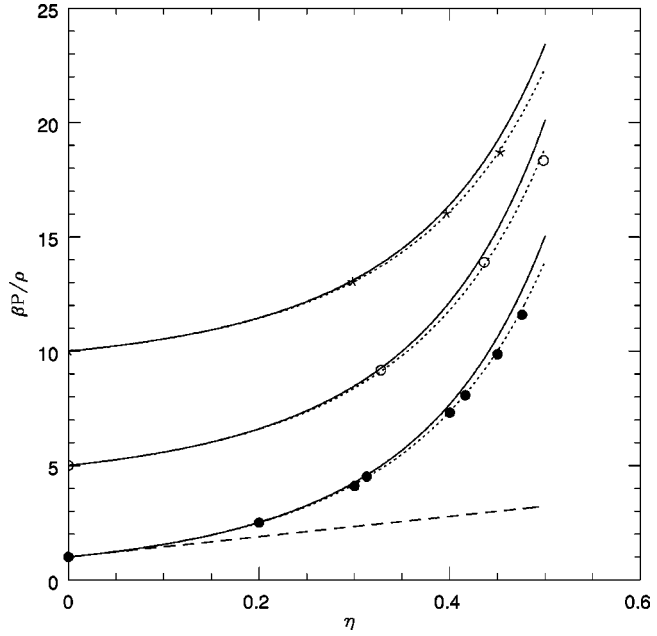

FIG. 1. The compressibility factors for mixtures of spherocylinders ($\sigma=1$ and $L=1$) and hard spheres ($\sigma=1$) as a functions of the total packing fraction η. The symbols are Monte Carlo results from Ref. [25]; the solid lines are for the SPT pressure [Eq. (23)] and the dotted lines for the Carnahan-Starling type approximation [15]. The upper curves have been shifted by 5 (10). The topmost data are for a hard sphere composition $x_1=0.7143$, the middle data for $x_1=0.2$, and the lowest data for $x_1=0.5$. The dashed curve is the second virial approximation [Eq. (25)].

A. Comparative study of the pressures

In order to test the accuracy of the GADCF for mixtures, it would have been nice to compare the structural data to that from another theoretical method (simulation or integral equations). As mentioned in Sec. II, such a comparison would be possible only if DCF's were available from integral equations techniques. This is not presently the case. Alternatively, one could indirectly test the accuracy of the DCF through the thermodynamical properties that can be derived from it, namely, the pressure, and compare with computer simulation results. Although such data are not available for spherocylinder mixtures, there are some Monte Carlo pressure data for spheres and spherocylinder mixtures [25] for equal diameters and cylinder length $L=1$. Although this is a small anisotropy, it nevertheless allows one to examine the extent of the validity the geometrical approximation. The pressure calculated from Eq. (23) is shown in Fig. 1 together with the Monte Carlo data for three different hard sphere densities ρ_1. We see that the agreement can be considered satisfying. In fact, it is quite similar to that obtained for single fluid systems. For the latter case, the agreement was considered quite remarkable even for elongation as large as 11 for rigid bodies, and 200 for freely jointed chains [17]. For curiosity we

have added the truncated pressure from Eq. (25), which is clearly not an acceptable approximation in this case. Indeed, Eq. (25) gives a compressibility factor $P/(\rho k_B T)$ that is *linear* in density, and its validity is then restricted to very small packing fractions.

Now, in order to test the range of accuracy of Eq. (25) versus that given by Eq. (23), in Fig. 2 we consider two different cases, where the second specie is treated at the SVCOA level. In Fig. 2(a) we consider an equimolar mixture of very elongated spherocylinders ($L_2=100$) in a spherical solvent ($L_1=0$) in one case, and in a liquid crystal solvent ($L_1=10$) in another case. The respective pressures are shown in Fig. 2(a) for several theories. We have also added the Carnahan Starling pressure that can be defined through the SPT variables [15], and can be seen to be indistinguishable from that given by Eq. (23). On the other hand, Eq. (25) merges with the two others only for very small packing fractions $\eta<0.002$, which was to be expected.

In the second example, [Fig. 2(b)], we consider a mixture of colloidal TMV (tobacco mosaic virus) in a typical liquid crystal. This example is taken from Ref. [10] and the dimensions of the two molecules are (the TMV is component 2) $\sigma_1=4.5$ Å, $L_1=600$ Å, $\sigma_2=180$ Å, and $L_2=3000$ Å. Reducing all units by σ_1, and keeping the same notations with $\sigma=1$, we have now $\sigma_2=40$, $L_1=133.33$, and $L_2=666.67$. In this case, we see that the second virial approximation does not compare very well with the SPT pressure [Eq. (23)]. We have also plotted a simplified version of P_O where the second virial coefficients are further simplified by taking the $L/\sigma\to\infty$ limit. The simplified virial coefficients then become $b_{2;\alpha\beta}=(\pi/4)L_\alpha L_\beta(\sigma_1+\sigma_2)/2$. These expressions, and the associated pressures, were often used recently [10,6], and we see here that they might not be the best approximations, as in this case they seem worse than the full second virial expression.

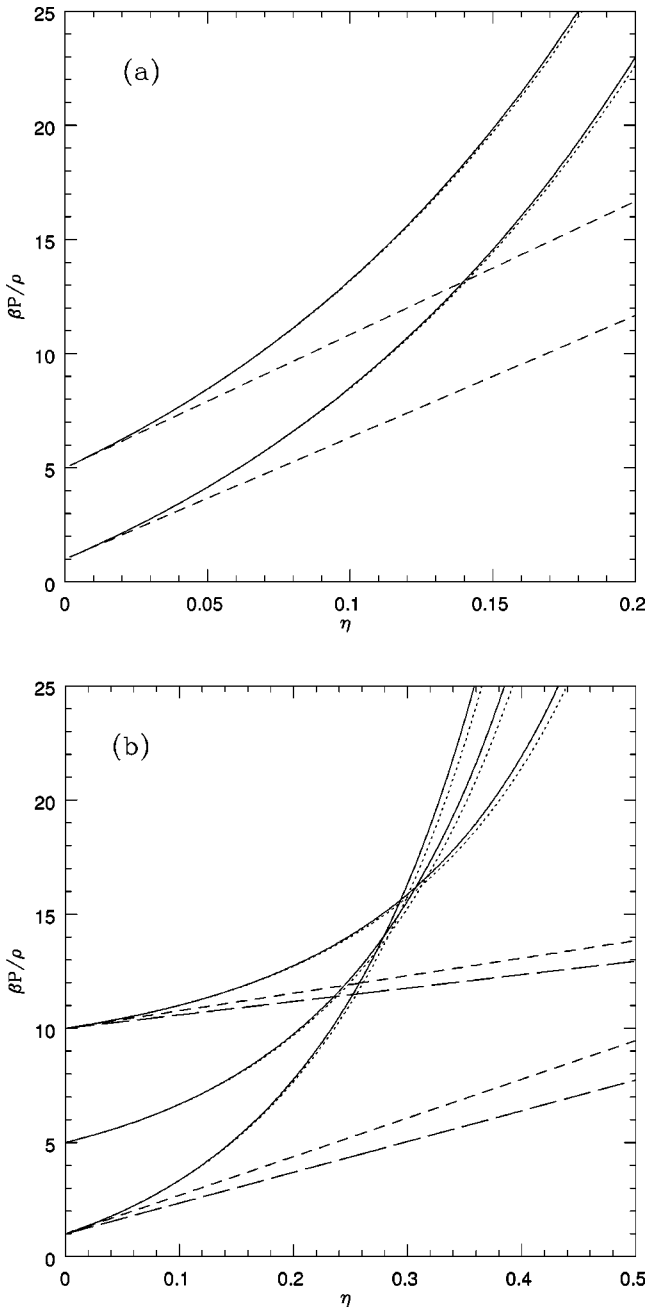

FIG. 2. (a) The compressibility factor for an equimolar mixture of spherocylinders with the same diameter $\sigma=1$. The solute cylinder length is $L_2=100$, and the solvent is a hard sphere: ($L=0$, bottom curve) and $L=10$ (top curve, data shifted by 5). The line symbols are as in Fig. 1. (b) The compressibility factor for a spherocylinder model of the mosaic tobacco virus ($\sigma_2=40$ and $L_2=666.67$) in a model liquid crystal solvent ($\sigma_1=1$ and $L_1=133.33$). The line symbols are as in Fig. 1. The long dashes as for the full Onsager limit.

B. Entropic demixing and orientational spinodal

Entropic demixing can be located by using the Gibbs free energy curvature criteria [Eq. (2)]. This criteria can be written in terms of the direct correlation functions, by using the definition of the partial structure factors [Eq. (8)] through the OZ equation (7) and the compressibility equation (24).

Following Biben and Hansen [3], we define the $\Lambda=x_1x_2(\partial^2[G/(Nk_BT)]/\partial x_1^2)_{N,P,T}$, and rewrite this expression by using Eqs. (2), (7), (8), and (24) in the term

$$\Lambda=\frac{\chi_T}{\chi_T^0}\det(\mathbf{I}-\tilde{\mathbf{C}}_0). \tag{27}$$

As one approaches the demixing region, from Eq. (9) we see that Λ from Eq. (27) will decay to zero. This expression is used in Fig. 3 to show the possibility of an entropic demixing for several mixtures, where the packing fraction of specie 1 is fixed at $\eta_1=0.3$, and that of specie 2 is varied between 0 and 0.4, values that are reasonably small packing fractions for a fluid. We recall that for a hard sphere the fluid region extends up to $\eta=0.49$. In any case, it seems reasonable to keep the total packing fraction below 0.5 in order to ensure a liquid phase. Different size and aspect ratios of the spherocylinders have been considered. We see that the general trend for demixing, at reasonable liquid type packing fractions, is that the thickness of the second specie must be large and the cylinder lengths long. To be more specific, Fig. 3 shows that for $\sigma_2=\sigma_1$ demixing never occurs regardless of

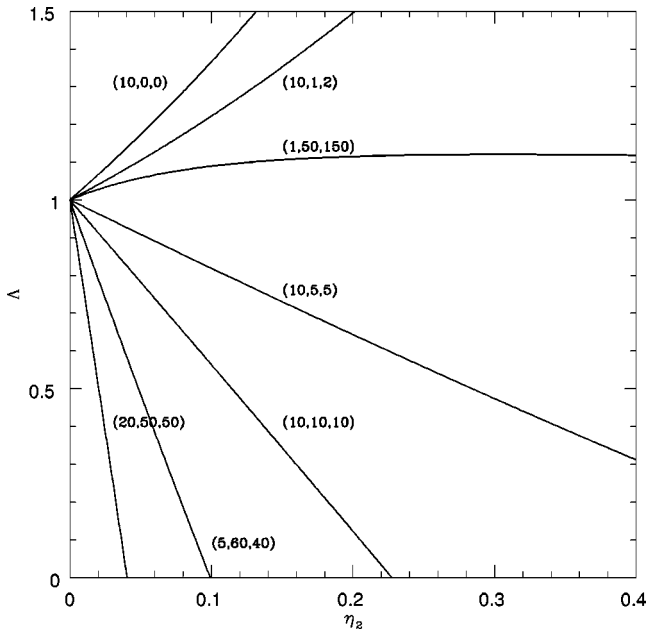

FIG. 3. The phase stability criteria Λ related to the free-energy convexity (see text) for several spherocylinder mixtures, at a fixed packing fraction of specie 1 ($\eta_1=0.3$). The numbers in parentheses are the dimensions of both species (σ_2, L_1, and L_2) (with the convention $\sigma_1=1$).

the rod lengths. The topmost curve also reveals the Percus-Yevick nature of the theory, signaling no demixing for spheres with a size ratio as large as 10. This trend also persists when the cylinders are short (second curve from the top). In order to see a turnover of the Λ curves, one must go to large diameters and long cylinders. But this is not a necessary condition, as indicated by the case with $\sigma_2=5$, but with very long cylinders of lengths $L_1=60$ and $L_2=40$. Although the general trends can be seen from the Λ curves, we cannot see properly how changing the densities of the solvent influences the solute. For a more global view, we must display spinodal curves.

One feature that cannot be seen from Fig. 3 is that, if the cylinders become very long, then they will likely tend to form an ordered phase at large packing fractions. The condition for orientational instability is also given by Eq. (9), or alternatively Eq. (18), but for $m=2$. For spherocylinders, using Eq. (18) together with Eqs. (10), (15), and (17) gives an analytical expression that cannot be further reduced. Therefore, we have solved for the zeros of this equation in terms of either variables (η_1, η_2) or (ρ,x_2).

We now examine the different cases that can be relevant or not for entropic demixing. For this purpose, we examine the quadratic form in Eq. (22). We seek physical density solutions for this equation, as $x=x_2$ varies between 0 and 1 (pure solvent and pure solute limits). In general, in view of Eqs. (20b) and (22), it will not be possible to tell if there is a demixing transition. Numerical investigation is necessary. But there are few cases where this can be done analytically.

1. Spherical solvent or spherical solute

We first consider the pure hard spheres mixture, in which case we recall that our approximation gives exactly the PY solution, thus leading to no demixing. In this case, we find that the quadratic equation [Eq. (22)] gives the following *negative* value for a possible demixing density as a function of the large spheres composition x:

$$\rho_S(x)=\frac{-3}{\pi[1+x(\sigma_2-1)]}. \tag{28}$$

This absurd result is clearly a consequence, and an illustration, of the inability of PY theory to predict phase separation for hard spheres mixtures.

We now consider a spherical solvent ($L_1=0$), when the solute particles are spherocylinders with arbitrary dimensions (we recall here our convention that $\sigma_1=1$ always). This case that can be resolved from Eqs. (20b) and (22). Direct inspection of the analytical result for Eq. (22) is not very helpful. Instead, we look at the values of ρ_S for $x=0$ and $x=1$, which we find to both be negative:

$$\rho_S(0)=\frac{-3}{\pi},\quad \rho_S(1)=\frac{-6}{\pi\sigma_2^2(L_2+\sigma_2)}. \tag{29a}$$

We now look for a change in sign of the denominator $D(x)$ of Eq. (22) and its derivative $D'(x)=dD(x)/dx$ for $x=0,1$. We find

$$\begin{aligned} D(0)&=16\pi^2,\\ D'(0)&=\pi^2\sigma_2^3(3L_2+4\sigma_2)(6L^2+9\sigma L_2+4\sigma_2^2),\\ D(1)&=\pi^2(32(\sigma_2^3-1)+3L_2^2(8\sigma_2^2-3)+48L_2\sigma_2^2),\\ D'(1)&=\pi^2(32\sigma_3(\sigma_2^3-1)+48L_2\sigma_2^2(3\sigma_2^3-1)\\ &\quad +6L_2^2\sigma(17\sigma^3-4)9L_2^2(4L_2\sigma_2^3+1)) \end{aligned} \tag{29b}$$

As $\sigma_2>1$ by convention, we see that $D(0)>0$ and $D(1)>0$, and similarly $D'(0)>0$ and $D'(1)>0$. In view of the particular form of Eq. (22), one sees that $\rho_S(x)$ will have the same sign for any x in the interval $[0,1]$, and hence, from Eq. (29a) ρ_s will always be negative. In other words, our theory predicts no demixing for arbitrary spherocylinders in a standard hard sphere solvent. However, this prediction seems strongly related to the PY nature of the theory, and we expect that simulation studies of thick spherocylinders in a hard sphere solvent should show an entropic demixing at reasonable fluid packing fractions.

Next we consider the mixture of a spherical solute immersed in a solvent of thin spherocylinders. The difference from the previous case is that we can now consider large spheres, whereas the diameter of the solvent spherocylinder is confined to $\sigma_1=1$ by convention. We will use the same method as in the previous case, as direct inspection of Eq. (22) again gives no useful information. We find that

$$\rho_S(0)=\frac{-12}{\pi(3L_1+4)},\quad \rho_S(1)=\frac{-3}{\pi\sigma_2^3}, \tag{30a}$$

and the denominator and derivatives at $x=0$ and 1 are

$$D(0)=\pi^2(3L_1+4)(6L_1^2+9L_1+4),$$

$$D'(0)=\pi^2[32(\sigma_2^3-1)+48L_1(\sigma_2^3-2)+6L_1^2(4\sigma_2^3-17) -9L_1^2(4L_1+\sigma_2^4)] \tag{30b}$$

$$D(1)=16\pi^2\sigma_2^6,$$

$$D'(1)=\pi^2\sigma_2^3[32(\sigma_2^3-1)+3L_1^2(3\sigma_2-8)-48L_1].$$

In this case, although the denominator remains positive, we see that the sign of the derivatives will depend on the size of the solute and the length of the cylinder of the solvent particle. However, for large L_1 it is likely that the derivatives remain positive, and hence that $\rho_S(x)$ has poles in the interval $[0,1]$, leading to situations different from Eq. (30a). This is exactly what we find numerically when the solvent cylinder length L_1 is larger than the solute size σ_2.

In the figures below, we plot the composition of solute $x=x_2$ vs the total packing fraction associated with the spinodal densities $\eta=\rho_S/[(1-x)V_1+xV_2]$ in the upper panel, and the associated pressures in the lower panel.

In Figs. 4(a) and 4(b) we show two cases where the spinodal demixing can occur. The pressure curves exhibit the typical U shaped curves, with a lower critical consolute point at the minimum. However, we also must confront the demixing with the orientational instability that can occur when the solvent particles are very long. In the figures, the orientational spinodal is plotted in dashed lines. In Fig. 4(a), for $L_1=50$ and $\sigma=10$, we see in the upper panel that the entropic demixing occurs at quite large packing fractions $\eta>0.338$, but that most of the demixing is buried above the orientational spinodal. In the very small region where demixing could occur ($0.45<x<0.60$), the packing fractions are already too large to expect a liquid phase.

We see that the pure solvent ($x=0$) is ordered at all packing fractions above 0.065, and that the further addition of spherical solute will shift the isotropic-nematic spinodal to higher packing fractions, as should be expected. This is a nice feature of the theory, which seems correctly built in the geometrical approximation of the direct correlation function for mixtures.

The spinodal pressures, $P_S^*=P\sigma_1^3/(k_BT)$, as computed from Eq. (23) with the corresponding spinodal densities, are displayed in the lower panel of Fig. 4(a). We see that possible entropic demixing can occur at same pressure for two different spherical solute composition (low and high $x=x_2$). In Fig. 4(b) a successful entropic demixing is shown for $L_1=50$, but when the solute size is larger $\sigma_2=20$. The upper panel shows quite clearly that there is a wide range of compositions ($0.05<x<0.45$) of the large spheres. Beyond this range, it is the orientational spinodal that will dominate the phase separation. However, this takes place at unrealistically high packing fractions ($\eta>0.8$). In such a case, we can reasonably expect the entropic demixing to occur in the disordered phase, but at very low solute compositions ($x=x_2<0.05$). The lower panel shows the pressures. The reason for

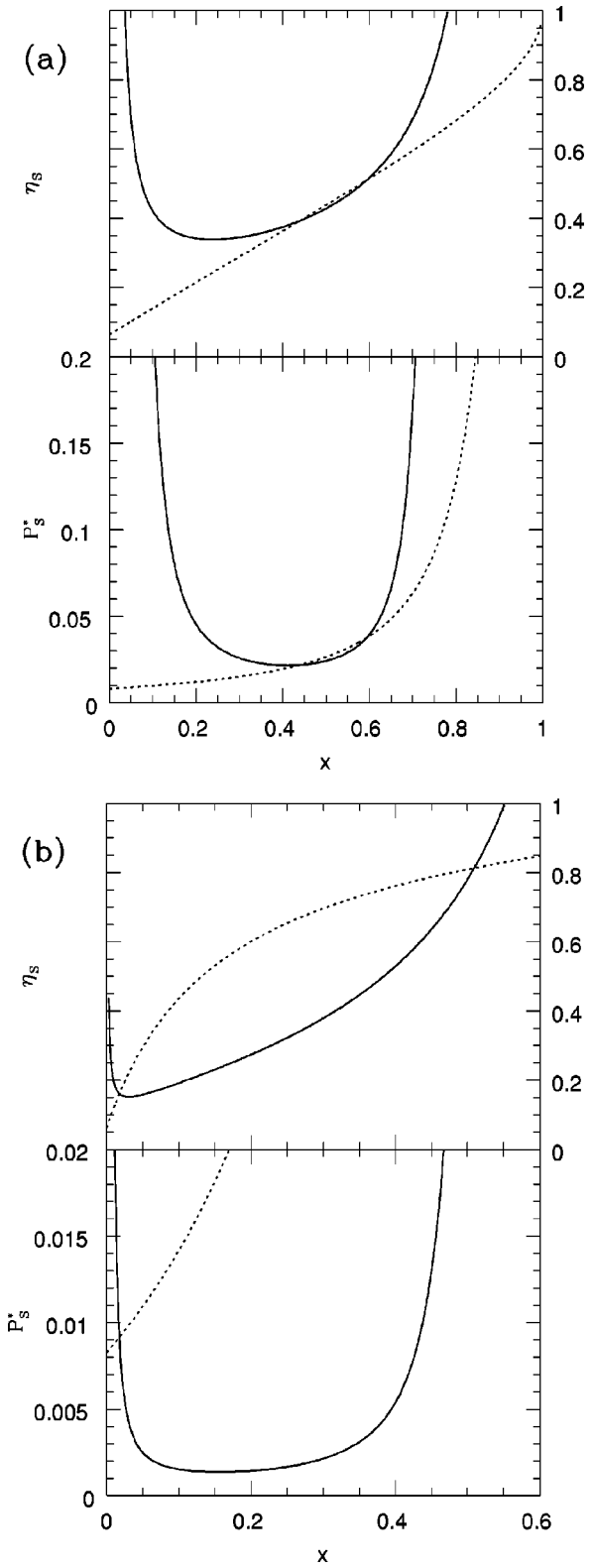

FIG. 4. (a) The entropic demixing spinodal packing fraction (upper panel) and corresponding pressure (lower panel) vs the solute composition $x=x_2$, for a mixture of a spherocylinder ($\sigma_1=1$ and $L_1=50$) and a hard sphere (HS) ($\sigma_2=10$). The full line is for the demixing spinodal, and the dotted curve for the orientational spinodal. (b) Same as in (a), when the HS solute size is increased ($\sigma_2=20$).

such small pressure values is related to the very small densities at which coexistence can occur. This is also related to the choice of units (scaling by the smallest diameter $\sigma_1 = 1$).

Finally, we also note that entropic demixing that is not masked by the orientation spinodal can also occur when $\sigma_2 > L_1$, for example $\sigma_2 = 80$ and $L_1 = 30$. In such a case, however, we find that this occurs only for very small solute compositions $x = x_2 < 0.03$. For $x = 0.03$, however, the total packing exceeds 0.95, the value at which orientational ordering is supposed to take over. We thus conclude that the mixture remains disordered in the entire fluid region. This is to be expected, since such a large spherical solute will certainly perturb the orientational ordering.

It is not possible to find a general analytical criteria for ''acceptable'' values of (σ_2, L_1), values which will show a fluid-fluid demixing, partly due to the numerical part involved in the calculation of the orientational spinodal. We will now turn to cases where both particles are true spherocylinders.

2. Equally thin spherocylinders mixture

The case where $\sigma_2 = \sigma_1 = 1$ and $L_1 \neq 0, L_2 \neq 0$ is also a case where the present theory does not predict demixing at all. Again, we first look at the solutions $\rho_S(x)$ at $x = 0$ and 1, which we find to be negative:

$$\rho_S(0) = \frac{-12}{\pi(3L_1 + 4)}, \quad \rho_S(1) = \frac{-12}{\pi(3L_2 + 4)} \tag{31a}$$

In addition, we find that the denominators of Eq. (22) for $x = 0,1$ do not change sign, and similarly for their derivatives:

$$\begin{aligned} D(0) &= \pi^2(3L_1 + 4)(6L_1^2 + 9L_1 + 4), \\ D(1) &= \pi^2(3L_2 + 4)(6L_2^2 + 9L_2 + 4), \\ D'(0) &= -3\pi^2(L1 - L2)(16 + 5L_2 + 6L_1L_2 + 29L_1 + 12L_1^2), \\ D'(1) &= -3\pi^2(L1 - L2)(16 + 5L_1 + 6L_1L_2 + 29L_2 + 12L_2^2). \end{aligned} \tag{31b}$$

Therefore this case leads to nonphysical negative demixing densities in the entire x range $[0,1]$, and hence fails to predict demixing for a mixture of thin liquid crystals. It is difficult to see if this prediction is a feature of the Percus-Yevick nature of the present theory, or if it a generic one. In view of the fact that it is necessary to go to large size ratios in order to find demixing for hard sphere mixtures, the present finding seems to be in good agreement. The authors are not aware of any experimental evidence of entropic demixing in liquid crystal mixtures in the isotropic phase, although it is not impossible that energetically favored demixing could occur. We leave this point open for future verification, most probably by computer simulation techniques.

3. General case

In the general case Eq. (22) is of no help from an analytical point of view, and it must be solved case by case numerically. We wish here to point out some of the general features.

First we consider the case of equal length cylinders, but with different thicknesses. The solute spherocylinder is now constrained to have the same cylinder length as the solvent, but larger thicknesses. We observe that for thicknesses smaller than 6, the orientational spinodal will always override the demixing spinodal, regardless of the cylinder length. From $\sigma_2 > 10$ it is possible to find demixing if L is large enough. Furthermore, the composition domain over which demixing can occur, shrinks toward small values when σ_2 becomes large at a fixed L value. Conversely, at a fixed σ_2 value, the demixing region increases with increasing L. Generally, as particles become larger, the demixing densities become very small (and consequently the associated pressures). Then the addition of large solute particles will push the spinodal densities toward lower values. But the total packing fraction increases as L increases.

The demixing of equal length spherocylinders have been investigated by Dijkstra and van Roj [6] with Gibbs ensemble computer simulation techniques. They also compared their results to calculations in the FOA. It is important to realize that computer simulations measure binodals, which are the equivalent of the phase coexistence curves. Conversely, the theories we discuss here predict spinodal curves. It is clear that the spinodal curves should be inside the corresponding binodal. The system simulated in Ref. [6] is for the parameters $\sigma_1/\sigma_2 = 0.1$ and $L = L_1 = L_2 = 15\sigma_2$. With our convention $(\sigma_1 = 1)$, this is equivalent to $\sigma_2 = 10$ and $L = 150$. In Fig. 5, we plot the spinodals corresponding to the present theory, together with those of the Onsager type theories and the binodals from the computer simulations. For an easier comparison, we have taken the same units as in Ref. [6], that is $\rho^* = \rho b$ and $p^* = Pb\sigma_2/(k_BT)$, where $b = \pi/4L^2$. We first notice that there is an appreciable difference between the SVCOA (dashed curves) and the FOA (dotted curves), which is in fact the reference theory in Ref. [10]. The density range at which demixing is predicted is between $0 < \rho\sigma_1^3 < 0.32 \times 10^{-4}$, and for such small densities that we expect that a second virial coefficient approach to be a good approximation. However, we observe that this is clearly not the case. In fact the x range over which the theories coincide is about $0 < x < 0.05$. Surprisingly, it is the FOA that is closer to the results from the GADCF. As the orientational spinodal is independent of the $L/\sigma \to 0$ limit in any of the Onsager type approaches, the two curves for the spinodal densities are identical. However, the corresponding pressures differ, as the FOA neglects the spherical caps contributions in the B_2 in Eq. (25). The binodals that one would associate with these curves should be outside and broader in shape, with one contact point with the corresponding spinodal curves; that would be the lower consolute critical point. Reference [5] contained an example of both such curves for hard sphere mixtures. As noted by Dijkstra [6], the critical composition predicted by the FOA, $x_2 \approx 0.2$, is in rather close agreement with that of the simulations. The GADCF predicts a smaller critical composition $x_2 \approx 0.14$. Of the three theories, it is the FOA that predicts a critical pressure closest to the simulation results. We note that the binodal from the simulations is very broad. But in the absence of free energy calculations, it is not possible to predict the true shape of the

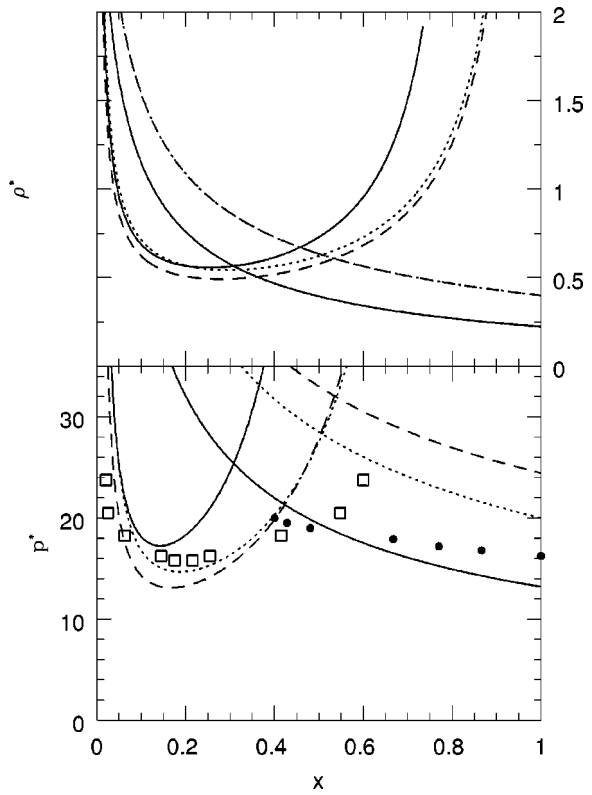

FIG. 5. The entropic demixing of a spherocylinder mixture of equal length $L=150$ and different thicknesses ($\sigma_1=1$ and $\sigma_2=10$). The densities in the upper panel are $\rho^*=\rho_S b$, and the pressures are $p^*=Pb\sigma_2/k_BT$ [$b=(\pi/4)L_1^2\sigma_1$]. Full lines are for the GADCF, dotted lines for the SVCOA, and dashes for the FOA. The U shaped curves are the demixing spinodals, and the monotonically decreasing curves (for increasing x) are orientational spinodals. The open cubes are the Gibbs ensemble demixing binodal from Ref. [6], and the filled dots for the orientational binodal are from the same reference.

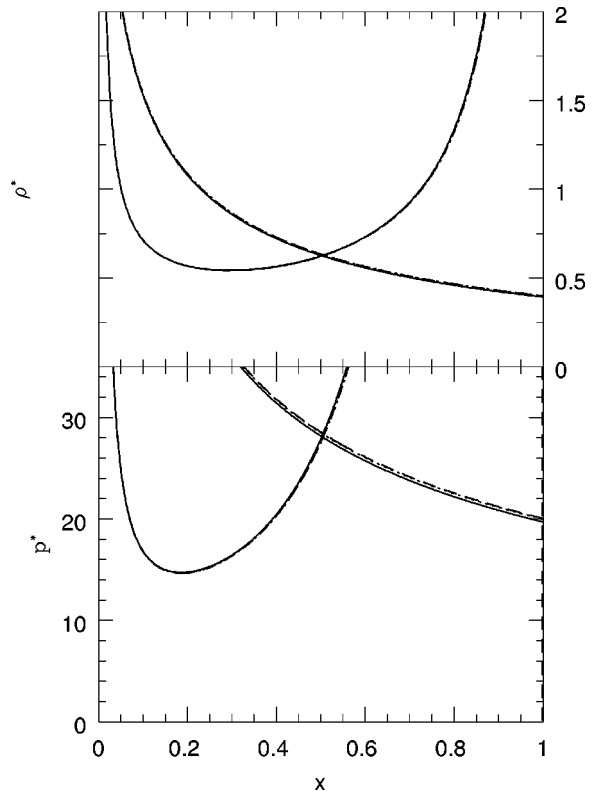

FIG. 6. The entropic demixing of spherocylinder mixtures in the quasi Onsager limit ($\sigma_1=1$, $\sigma_2=10$, and $L_1=L_2=10^4$). The line symbols and units are used as in Fig. 5.

binodal associated with the GADCF for the present case. In Ref. [6], binodals of the FOA (from their unpublished Ref. [25]) were plotted, and these curves were below the binodal of the simulations. In view of this one might expect that the binodals of the GADCF might be above and closer to the simulation results than the current spinodal. The comparisons of the orientational spinodals are easier, as the isotropic-nematic transition is weakly first order. Hence we expect the spinodal to lie closer to the binodal in this case. However, this is not the case for the Onsager theory, which predicts a large density gap [1]. In general the orientational spinodal from the GADCF is closer to the simulation results than the two others. However, in Ref. [6], the binodals associated with the FOA are again below but quite close to that from the simulations. We observe that the geometrical theory strongly underestimates the isotropic-nematic spinodal for the pure solute ($x=1$), a feature that was already noticed [15].

In order to test the degree of convergence of the three theories, in Fig. 6 we consider the case of very long spherocylinders. We note that the FOA is independent of the individual cylinder lengths L_1 and L_2, and depend only on their ratio [10]. The corresponding curves in Fig. 5 are then for infinitely long cylinders, as opposed to the two other theories, and it is quite surprising to see that all three curves are quite close to each other. In order to further test the adequacy of the theories to fit the FOA, in Fig. 6 we plot the spinodal densities and pressures for $\sigma_2=10$, but with $L_1=L_2=L=10^4$. We observe that all three curves indeed merge as they should. In fact they have still some small differences that can be observed for larger densities and pressures. They merge totally for $L\approx 10^6$. At $L=10^3$, for example, the curves are well separated for $x>0.3$, and merge relatively well for smaller x values. In view of these results, we conclude that the agreement in Fig. 5 between the FOA and the simulations seems fortuitous.

The influence of the cylinder length of the critical point was also studied in Ref. [6], namely, when L/σ_2 varies at fixed $\sigma_2=10$. The comparison with the GADCF in Fig. 7 shows that, as L/σ_2 becomes smaller, the discrepancies in the spinodal increase in a dramatical fashion. The theory indicate that the critical points move to higher pressures and lower compositions, whereas the simulations show no change at all in the position of the critical points. This strong discrepancy certainly deserves further investigation. It seems that the predictions of the GADCF are more natural, as shorter particles will push the demixing toward lower composition regions and higher pressures and packing fractions. Eventually, for even shorter spherocylinders, the demixing will disappear, as it will occur only at unphysically high pressures and densities. Hence one would also expect the

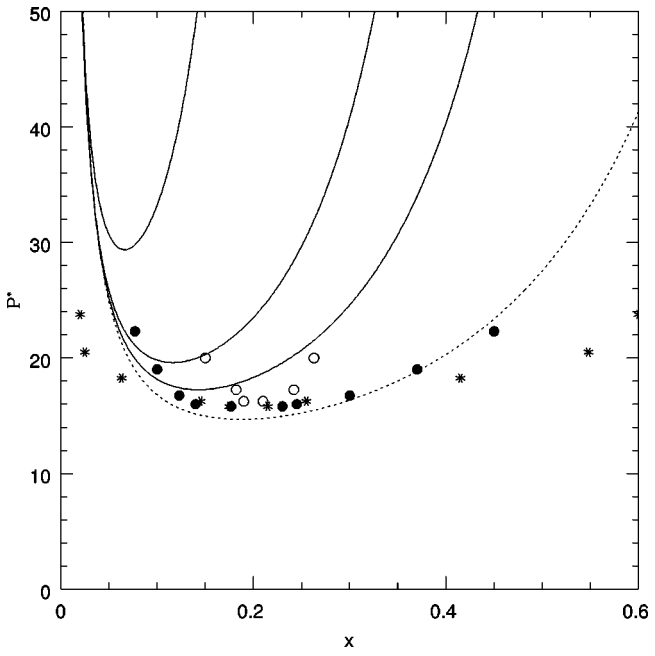

FIG. 7. The entropic demixing of equal length spherocylinders mixtures of different cylinder lengths ($\sigma_1=1$, $\sigma_2=10$, and $L=L_1=L_2$). The lines are for the GADCF (topmost curve for $L=30$, middle curve $L=80$, and lower curve for $L=150$. The dotted line is for the FOA. The symbols are Gibbs ensemble simulations binodals from Ref. [6] (open dots $L=30$, filled dots $L=80$, and stars $L=150$). The units are as in Fig. 5.

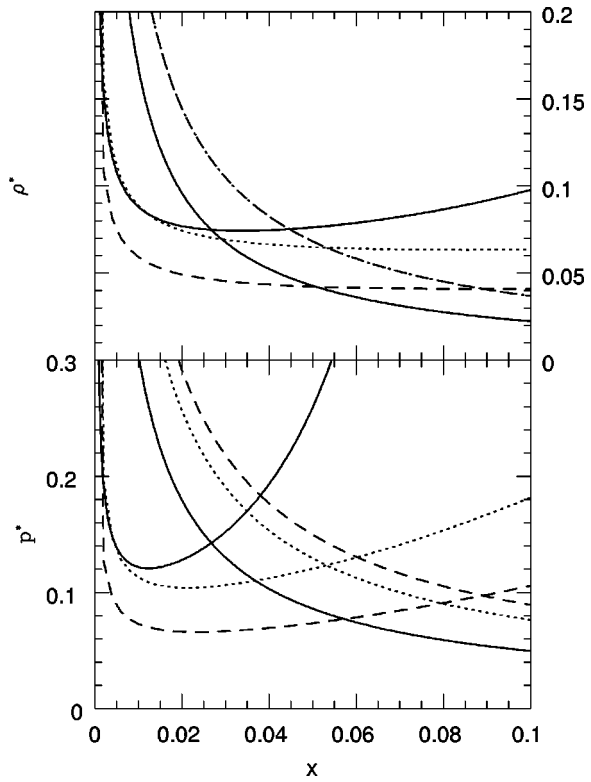

FIG. 8. The entropic demixing of model TMV in a liquid crystal. The parameters are the same as in Fig. 2(b). The line symbols and units are as in Fig. 5.

critical point to follow a similar trend. The simulations however agree with the GADCF only in that they both predict a narrowing of the spinodals and binodals with decreasing cylinder lengths. The FOA is shown by a single dotted curve, and is seen to be independent of L/σ_2.

For the case of unequal cylinder lengths, we consider again the TMV example of Sec. III A. There is a possible demixing in this mixture that occurs at very small isotropic TMV compositions. This is shown in Fig. 8, where the three theories are compared for both the spinodal densities and pressures. The trends are very much similar to those observed in Fig. 5. The GADCF has the narrowest spinodal curve and the highest critical pressure. We also note that, despite the quite long cylinder length of the TMV, the Onsager regime is clearly not reached. In view of what is found here and what was described in Sec. III B 1, we conjecture that entropic demixing is more likely to be observable when a nonorienting fluid is added to a liquid crystalline solvent. In such a case, the orientational spinodal can be suppressed if the solute shape is close to spherical. If both fluids are liquid crystalline materials, then demixing could occur only in a very narrow low composition window for the larger molecules. This needs to be confronted with experiments, and eventually computer simulations.

C. A very particular case: Spherocylinders in needles

The case of spherocylinders immersed in a fluid of hard needles was also investigated by Dijkstra and van Roij [6] using Gibbs ensemble techniques. The hard needle fluid in three dimensions is very peculiar as it has no excluded volume, thus it can be packed to infinitely high densities. Hence such a fluid will never order as it behaves as a fluid of noninteracting ideal particles. However, when a particle is added to it, there will be an excluded volume between the two components. Because of the geometrical simplicity of the interactions, this case can also be described by the GADCF. The fundamental measures of the needle are reduced to the mean radius, which from Eq. (26) is $R_m=L/4$, where L is the length of the needle. We see from Eq. (14) that the second virial coefficient of the needle is zero, and that the DCF is identically zero, indicating the total absence of interactions between needles. The other partial DCF's c_{12} and c_{22} are nonzero, and the needle will contribute to their GADCF through the mean radii only.

We can thus calculate the demixing spinodal line using Eq. (22). The results are shown in Fig. 9 for $L_1=L_2=150$ and $\sigma_2=10$. The general trends are again quite similar to that observed for both Figs. 5 and Fig. 6. We note that the critical spherocylinder compositions found by the GADCF and FOA are in narrow agreement with the simulations results, that is $x_c\approx 0.11$. This value cannot be reached through second virial coefficient only. We also note that the orientational spinodal is somewhat closer to that of the GADCF.

A particular case of this type of mixture was also studied by Gibbs ensemble techniques, namely, the mixture of hard rods and spheres [26]. In this case a very simple approximation for the free energy, that was built from the Carhanan-Starling free energy together with the Onsager approxima-

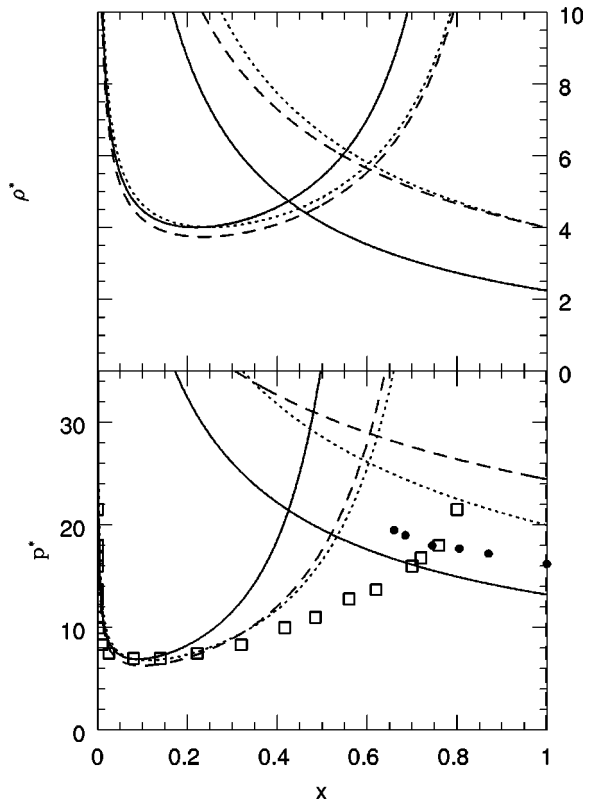

FIG. 9. The entropic demixing of a spherocylinder and a needle mixture. The symbols are the from Ref. [6]. All the symbols and units are as in Fig. 5.

tion for the needles, was shown to predict binodals in very good agreement with that from the simulations. As a free energy is built in the GADCF, we also expect to see similar agreement, particularly in view of the proximity of the GADCF spinodal to the binodals from the simulations.

IV. CONCLUSION

In this work, we have presented an application to mixtures of the geometrical approximation for the direct correlation functions derived in our previous work [15]. Although we did not compare the DCF itself to other theoretical approaches, namely, to integral equations results we showed that the SPT pressure, that is consistent with the GADCF, is in quite good agreement with Monte Carlo simulation results, for the case of a mixture of hard spheres and short spherocylinders. The GADCF was essentially used to show that entropically driven phase separation could occur in a variety of mixtures of spherocylindrical particles. It was concluded that a mixture of liquid crystalline materials and large solutes is the most favored candidate. Our analysis shows that a sufficiently large solute can preempt the orientational ordering of the solvent over a notable solute composition range, for the case where the solute is a nonordering fluid. This type of mixture is frequently encountered in experimental situations, but the *athermal* demixing condition that we describe here is a more demanding condition. Such condition are generally met in colloidal liquid crystals. Although some experiments on silica particles that illustrate demixing of hard spheres mixtures [27] are possible, we are not aware of a similar situation for nonspherical particles.

The main testing ground remains computer simulations, which pose formidable challenges when the size ratios are very large. The few comparisons between theory and simulations shown in the present work indicate a convincing agreement between theoretical spinodals and experimental binodals. However, these simulations are done for situations tailored to fit the Onsager limits, in order to test theories built at that level of approximation. It is not the most desirable test for the GADCF, which we believe should be more accurate, particularly for particles with moderate aspect ratios. The theoretical considerations from Ref. [26], that are somewhat closer to the GADCF, indicate that the latter should provide a better ground for predicting entropic demixing.

The GADCF fails to predict entropic demixing in three cases, namely, for hard sphere mixtures, for the more general case of spherocylinders immersed in a solvent of smaller spheres, and finally for equally thin spherocylinders. From what is known for hard spheres, the second case should be a candidate for entropic demixing, and the failure of the GADCF here reveals the PY nature of the theory. On the other hand, it would certainly be worth testing the prediction of integral equations, including the PY approximation, concerning entropic demixing in nonspherical hard particles. It is known that the PY theory predicts entropic demixing for positive nonadditive diameters [28]. In this respect, if one considers a mixture of nonspherical particles as effective spherical particles, the corresponding effective diameters will most likely be larger than the smaller size of the particles. Thus, in the absence of ordering tendencies, which means when particles are locally disordered, one might approximate the interactions as nonadditive hard sphere interactions. On this basis, one would then expect the PY theory to predict entropic demixing for such mixtures, and it might also explain the results that are found herein for the GADCF. Such an argument, however, does not account for the demixing that is found when both fluids are ordering ones, as most of the nearest neighbor contacts are truly additive in this case.

Finally, in view of the fact that the GADCF is PY like, it is quite probable that the boundaries of the demixing regions that are predicted from this theory are most likely conservative predictions. If demixing shoud occur, it will probably occur within the range of parameters predicted by the GADCF, and even at lower values. In this sense we can argue that the demixing densities predicted by the GADCF, for a fixed set of molecular parameter, are most likely upper bounds to that can be deduced from more complete (in a diagrammatic sense) theories. This argument is supported by Figs. 5 and 9 in particular, where on sees that spinodals from the GADCF are well above the binodals from the simulations.

Considering future investigations, it would be interesting to test the present theory for other convex body mixtures. In particular, entropic effects in mixing platelike particles, cutspheres for example, and spherical or rodlike particles must be quite different. It would also be interesting to analyze the influence of the shapes. In this respect, it would be of impor-

tance to extend the GADCF into ordered phases, so that the influence of entropic effects on the ordering can be also accounted for. On this subject also, only second virial coefficient theories were provided in recent years [26,30]. A first elementary step in this direction would be to calculate the entropic effects in rigidly ordered fluids. Preliminary investigations indicate that entropic driven demixing can also destabilize such types of mixtures.

APPENDIX: ADDITIVE HARD SPHERE DEMIXING IN THE SECOND VIRIAL COEFFICIENT APPROXIMATION

The additive hard sphere virial coefficient is for mixtures $B_{2;\alpha\beta}=\pi/12(\sigma_\alpha+\sigma_\beta)$. At the lowest density expansion approximation one has $\tilde{c}^{000}_{\alpha\beta}(k=0)=-2B_{2;\alpha\beta}$, and this expression can be inserted into Eq. (18) in order to find the spinodal density. Surprisingly, the corresponding ρ_s is a positive function in the whole interval of x [0,1], unlike the PY case for which it is negative [see Eq. (28)]. It is possible to compute the critical composition of the large spheres (with diameter σ) by calculating the single minima of $\eta_s(x)$ in this x interval. This critical value is

$$x_c=\frac{1}{1+\sigma^3}. \tag{A1}$$

The corresponding consolute critical density is given by

$$\rho_c=\frac{6(1+\sigma)[8\sigma^3(\sigma^2-\sigma+1)+(1+\sigma)^2(1+\sigma^2)\sqrt{\sigma^3}]}{\pi\sigma^3(\sigma-1)^2(\sigma^4+8\sigma^3+30\sigma^2+8\sigma+1)}. \tag{A2}$$

In order to have a fluid mixture, that is, when $\eta<0.5$, one needs at least the condition $\sigma\geqslant 2.95$. For $\sigma=5$ and a packing of small spheres of $\eta_s=0.3$, the minimal large sphere packing fraction for demixing is $\eta_L\approx 0.015$, which is seen to be quite small, when compared to values obtained from integral equations (see Sec. I). This demixing tendency at the SV-COA level of approximation is stronger than for any other integral equations. It is quite interesting to see that the PY theory that has the correct B_2, is incapable of producing a demixing. Coussaert and Baus [5] found that it was necessary to include up to a fifth virial coefficient in the PY equation of state to trigger demixing, which, however, was now found to occur at all size ratios.

[1] L. Onsager, Ann. N.Y. Acad. Sci. **51**, 627 (1949).
[2] J.L. Lebowitz and J.S. Rowlinson, J. Chem. Phys. **41**, 133 (1964).
[3] T. Biben and J.P. Hansen, Phys. Rev. Lett. **66**, 2215 (1991).
[4] A. Perera (unpublished).
[5] T. Coussaert and M. Baus, Phys. Rev. Lett. **79**, 1881 (1997); J. Chem. Phys. **109**, 6012 (1998).
[6] M. Dijkstra and R. van Roij, Phys. Rev. E **56**, 5594 (1997).
[7] P. Bolhuis and D. Frenkel, J. Chem. Phys. **106**, 666 (1997).
[8] A. Perera and G.N. Patey, J. Chem. Phys. **89**, 5861 (1988).
[9] H.N.W. Lekkerkerker, Ph. Coulon, and R. van Der Haegen, J. Chem. Phys. **80**, 3417 (1984).
[10] R. van Roij and B. Mulder, Phys. Rev. E **54**, 6430 (1996).
[11] R. van Roij and B. Mulder, J. Phys. II **4**, 1763 (1994).
[12] J.A. Cuesta, C.F. Tejero, H. Xu, and M. Baus, Phys. Rev. A **44**, 5306 (1991).
[13] J.A. Cuesta, Phys. Rev. Lett. **76**, 3742 (1996).
[14] M. Dijkstra, D. Frenkel, and J.P. Hansen, J. Chem. Phys. **101**, 3179 (1994).
[15] A. Chamoux and A. Perera, J. Chem. Phys. **104**, 1493 (1996).
[16] A. Chamoux and A. Perera, J. Chem. Phys. **108**, 8172 (1998).
[17] A. Chamoux and A. Perera, Mol. Phys. **93**, 649 (1998).
[18] A. Chamoux and A. Perera, Phys. Rev. E **58**, 1933 (1998).
[19] L. Blum and A.J. Torruella, J. Chem. Phys. **56**, 303 (1972).
[20] P.H. Fries and G.N. Patey, J. Chem. Phys. **82**, 429 (1985).
[21] J.P. Hansen and I.R. McDonald, *Theory of Simple Liquids* (Academic, London, 1986).
[22] A. Perera, P.G. Kusalik, and G.N. Patey, J. Chem. Phys. **87**, 1295 (1987).
[23] J.G. Kirkwood and F.P. Buff, J. Chem. Phys. **19**, 774 (1951).
[24] A.B. Bhatia and D.E. Thornton, Phys. Rev. B **2**, 3004 (1970).
[25] T. Boublík and I. Nezbeda, Collect. Czech. Chem. Commun. **51**, 2301 (1986).
[26] P. Bolhuis and D. Frenkel, J. Chem. Phys. **101**, 9869 (1994).
[27] J.S. Duijneveldt, A.W. Heinen, and H.N.W. Lekkerkerker, Europhys. Lett. **21**, 369 (1993).
[28] D. Gazzillo, J. Chem. Phys. **95**, 4565 (1991).
[29] G.J. Vroege and H.N.W. Lekkerkerker, J. Chem. Phys. **97**, 3601 (1993).
[30] Y. Mao, M.E. Gates, and H.N.W. Lekkerkerker, J. Chem. Phys. **106**, 3721 (1997).